Glassy dynamics and equilibrium state on the honeycomb lattice: Role of surface diffusion and desorption on surface crowding

Shaghayegh Darjani,[1,2] Joel Koplik,[3,*] Vincent Pauchard,[1] and Sanjoy Banerjee[1,†]

[1]*Energy Institute and Department of Chemical Engineering, City College of New York, New York 10031, USA*

[2]*Benjamin Levich Institute and Department of Chemical Engineering, City College of New York, New York 10031, USA*

[3]*Benjamin Levich Institute and Department of Physics, City College of New York, New York 10031, USA*

(Received 6 November 2020; accepted 21 January 2021; published 8 February 2021)

The phase behavior and adsorption kinetics of hard-core particles on a honeycomb lattice are studied by means of random sequential adsorption with surface diffusion. We concentrate on reversible adsorption by introducing a desorption process into our previous model and varying the equilibrium rate constant as a control parameter. We find that an exact prediction of the temporal evolution of fractional surface coverage and the surface pressure dynamics of reversible adsorption can be achieved by use of the blocking function of a system with irreversible adsorption of highly mobile particles. For systems out of equilibrium we observe several features of glassy dynamics, such as slow relaxation dynamics, the memory effect, and aging. In particular, the analysis of our system in the limit of small desorption probability shows simple aging behavior with a power-law decay. A detailed discussion of Gibbs adsorption isotherm for nonequilibrium adsorption is given, which exhibits a hysteresis between this system and its equilibrium counterpart.

DOI: 10.1103/PhysRevE.103.022801

I. INTRODUCTION

The phase behavior and dynamics of adsorption in two-dimensional systems are key aspects of many current research areas such as phase transitions in amphiphilic monolayers [1], emulsion stability due to particle adsorption at interfaces [2–4], particle self-assembly into clusters [5–8], chemisorption on metal surfaces [9,10], and the melting at an interface [11,12].

Understanding the approach to the equilibrium state and the kinetics of adsorption are of great interest, particularly in separation and filtration, where both desorption and adsorption are present. Models accounting for desorption have also been used in vibrated granular systems [13,14], and in the adsorption of asphaltenes at toluene/water interfaces [15]. Further examples of the relevance of desorption occur in response to changes in experimental conditions, such as changing the pH of a solution, [16–18], rinsing with solvent or buffers [19,20], variations in temperature [21], and the addition of surfactants [13].

The Langmuir model [22] has been widely used to describe the adsorption behavior of reversible systems [1,23,24]. However, the Langmuir model has limitations: it fails to provide satisfactory predictions for systems composed of interacting particles [25–27] and when the adsorbate is larger than the adsorption site [27,28]. These deficiencies of the Langmuir model are addressed by the random sequential adsorption (RSA) and lattice gas models, which describe the adsorption kinetics and equation of state (EOS) of a monolayer, respectively. It is worth noting that, if the adsorption does not follow the Langmuir model, the adsorption properties and EOS become sensitive to the underlying lattice geometry such as square [29,30], triangle [31,32], and honeycomb lattices [33,34].

In the RSA model, molecules or particles which are larger than the adsorption sites are sequentially added at random to an initially empty surface, with the restriction that overlaps are forbidden. As the coverage increases, the free area left for further adsorption decreases, not only because of the sites occupied by previously adsorbed molecules but also because vacancies can be too small to allow adsorption without overlap. In the absence of surface diffusion or desorption, the adsorption process rapidly slows down and coverages only asymptotically approaches the jamming limit, equivalent to random maximum packing. In this limit, the jamming coverage depends on the lattice structure, the size and shape of the adsorbed particles [33,35]. However, several physical processes involve both adsorption and desorption, and here the system may stabilize in an equilibrium state below the maximum packing. In this situation, the RSA model with the addition of a desorption process has been used in the literature to study ion binding in Langmuir monolayers [16], the dynamics of ligand-substrate binding [36], the adsorption of fibrinogen molecules [37], and the decoration of microtubules with dimeric kinesin molecular motors [36]. All of these processes can be described via the simple RSA model at their early stage, while at a higher coverage stage detachment and reattachment of species plays a major role. It has been observed experimentally that the relaxation timescale of adsorbed particles, due to their rearrangement on the surface, can

*jkoplik@ccny.cuny.edu
†banerjee@ccny.cuny.edu

be comparable to the deposition timescale [38]. Diffusional relaxation on the surface leads to a denser monolayer with a more ordered configuration where the steric hindrance effects of previously adsorbed particles slows the process at the later stages [39].

The lattice gas model is a statistical mechanical approach to describe adsorbate configurations which, among other features, exhibits a phase transition at high surface coverage. This approach has been used to study phase transitions of photoexcited Rydberg gases [40], the self-assembly of isophthalic acid on graphite [41], the adsorption of selenium on a nickel surface [9], and the chemisorption of oxygen on palladium [42]. Although many versions of the lattice gas model have been studied in the literature, only the single case of a triangular lattice with first neighbor exclusion has an exact solution, given by Baxter [43]. For all other variants, a number of lattice gas methods have been developed over the years based on various approximations: the matrix method of Kramer and Wannier [44–50], the density (or activity) series expansion method [44,45,51–55], the generalized Bethe method [56–58], Monte Carlo simulations [49,59–63], the Rushbrooke and Scoins method [64], and fundamental measure theory [65]. Despite all of these efforts, the lattice gas model has not provided the adsorption kinetics of the system, and instead the main focus has been the EOS and the nature of phase transitions.

To combine the advantages of the RSA and lattice gas models we previously developed an alternative method, the RSAD model, to derive the EOS of two-dimensional nondesorbing hard-core particles based on kinetic arguments and the Gibbs adsorption isotherm on a triangular lattice [66,67]. One of the advantages of the RSAD model is its ability to locate the equilibrium state, ensuring that adequate thermalization had occurred and that finite-size effects are negligible. In the RSAD model, surface diffusion is introduced in parallel with adsorption so that vacancies large enough to adsorb further particles are both created and annihilated. When diffusion is sufficiently large, the size distribution of vacancies no longer depends on the history of adsorption (the positions where the adsorbates first arrived on the substrate) but only on the fractional surface coverage [68]. Note that, in this model, the potential energy is effectively infinite for particle overlap and zero otherwise, so that the system can therefore be considered as athermal [50,62,66]. Our results show that the RSAD model can be used as an equilibrium model where the EOS, the phase-transition coverage, and the nature of this transition are all in excellent agreement with the only available model with an exact solution in the literature [43].

Our past work on the RSAD model focused on irreversible adsorption of equilibrium states, but in this paper we substantially extend our previous RSAD approach by incorporating a desorption process and further explore the dynamics far from equilibrium. An important motivation is the experimental observation that when the relaxation timescale is much smaller than the experimental time-window, a system may evolve out of equilibrium [2,16,69]. In the remainder of this section we review the theoretical basis for the method and discuss the numerical implementation in Sec. II. A detailed discussion of our findings for both equilibrium and nonequilibrium systems is given in Sec. III and we summarize the paper in Sec. IV.

II. SIMULATION DETAILS

In the RSAD approach, for a two-dimensional lattice gas in equilibrium with a three-dimensional solution of adsorbate molecules, the equality of chemical potential throughout the system leads to

$$d\Pi = kT\frac{\Theta}{A_a}d\ln C. \tag{1}$$

Here, Π is the surface pressure, T is temperature, k is Boltzmann's constant, A_a represents the interfacial area covered by a single adsorbate molecule, Θ is the fractional surface coverage, and C is the concentration of the (three-dimensional) solution. Integrating the above equation gives:

$$\int_0^{\Theta}\frac{\Theta}{C}\frac{\partial C}{\partial\Theta}d\Theta = \frac{A_a}{kT}\Pi, \tag{2}$$

from which we see that knowledge of the adsorption isotherm, the relationship between $C(\Theta)$, bulk concentration, and fractional coverage, enables one to calculate the EOS, $\Pi(\Theta)$.

The adsorption isotherm, in turn, can be obtained through kinetic arguments. At equilibrium the rates of adsorption and desorption of molecules are equal:

$$K_aC(1-\beta(\Theta)) = K_d\Theta, \tag{3}$$

where K_a and K_d are the adsorption and desorption rate constants, respectively, and $\beta(\Theta)$ is the "blocking function," the fraction of the surface area, which is excluded from further adsorption by already-adsorbed molecules. Solving for C and inserting the resultant expression into the integral version of the Gibbs adsorption isotherm yields

$$\int_0^{\Theta}[1-\beta(\Theta)]\frac{\partial}{\partial\Theta}\left[\frac{\Theta}{1-\beta(\Theta)}\right]d\Theta = \frac{A_a}{kT}\Pi. \tag{4}$$

Thus, the blocking function is the only information needed to calculate the EOS, and we have shown previously [66,67] that, for lattice gases, the blocking function can be precisely extracted from RSAD simulations. From the definition of the adsorption rate, used above to define adsorption equilibrium, the blocking function can be extracted from the numerical simulations through the derivative of surface coverage with respect to time:

$$\frac{\partial\Theta}{\partial t} = \frac{K_l}{1+K_l}[1-\beta(\Theta)] - \frac{\Theta}{1+K_l}, \tag{5}$$

where $t = nA_a/A$, n is the number of attempts, A is the total number of sites, and $K_l = K_aC/K_d$. The blocking function can be further obtained from the rebuttal rate of adsorption attempts. In the absence of desorption ($K_l = \infty$), with highly mobile particles, the system can reach the full coverage. For the system of nondesorbing particle in equilibrium, Eq. (5) reduces to

$$\frac{\partial\Theta}{\partial t} = 1-\beta(\Theta). \tag{6}$$

The blocking function in Eq. (6) is obtained from the adsorption or desorption method described later in detail.

The adsorption of hard-core molecules with first-neighbor exclusion on the honeycomb lattice involves the adsorption of molecules covering two adsorption sites (see Fig. 1). Here, we

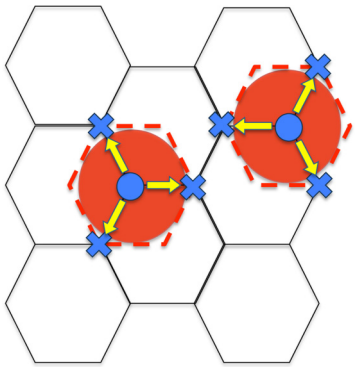

FIG. 1. Honeycomb lattice with first-neighbor exclusion where each adsorbate covers two sites identified by red circles. The center of the adsorbate is represented by a blue circle, arrows indicate possible displacements of particles, and the blue crosses represent the sites where the center of other particles are not allowed to occupy.

employ two complementary methods as described in our previous works [66,67]: an "*adsorption method*," which begins from an empty lattice, and a "*desorption method*," which begins with a full lattice and progressively decreases coverage. In the *adsorption method*, molecules or particles are progressively added to an initially empty $d \times d$ lattice surface where a periodic boundary condition is used to ameliorate finite-size effects. The only restriction is that overlap is not allowed; an assumption based physically on short-range electrostatic repulsion. For each adsorption attempt, a random position (x, y) is selected representing the center of mass of the particle. If the selected site and its neighbors are empty, adsorption is accepted, otherwise, it is rejected. Diffusion, the simultaneous movement of particles, is introduced sequentially with a predefined ratio D between the number of diffusion attempts and the adsorption attempt: For $D = 3$ each adsorption is followed by three diffusion attempts, etc. For each diffusion attempt, a previously adsorbed particle and a direction for the displacement of the particle are selected randomly; yellow arrows in Fig. 1 illustrate the possible directions. If moving the center of mass of the particle to the next node along this direction does not violate the nonoverlap condition, diffusion is accepted; otherwise, it is rejected. It is worth noting that, in the RSAD model, when diffusion is fast enough, the surface layer is at internal equilibrium (even during transient adsorption) and the blocking function can be considered as a state function.

For the *desorption method*, the lattice is initially full. In this method, two particles are randomly selected and removed. Then one adsorption attempt and D diffusion attempts are performed, until one particle is successfully deposited, following the same procedure as for the *adsorption method*. The choice of the sequence (two desorption events followed by one adsorption) is arbitrary but answers the need at each time step to decrease coverage and add at least one particle to calculate the adsorption rate. Note that desorption method is another way to calculate the adsorption rate in a reverse order.

For both adsorption and desorption methods, the blocking function is extracted from the rebuttal rate of adsorption attempts. Five hundred independent runs are performed, and an ensemble average is used to reduce the noise arising from the numerical calculation of the derivative of the coverage. The blocking function is fit with a polynomial function before using it to generate the adsorption isotherm. The latter is inserted into the Gibbs adsorption isotherm equation to obtain the EOS.

In the current study, we have additionally incorporated desorption into the system aiming to validate our hypothesis that the correct evolution of fractional surface coverage and its equilibrium value, as well as the blocking function, can be faithfully predicted for systems with different values of K_l, provided we have the knowledge of the system with $K_l = \infty$. In this method, at each attempt, we randomly choose a site with a predefined value of K_l. The desorption attempts are carried out as follows: If a chosen site lies inside the adsorbed particle (inside the red circle illustrated in Fig. 1), that particle is removed. Otherwise, we choose randomly one of the three neighboring sites and if that belongs to the center of mass of an adsorbate, we remove that particle. It is worth noting that, in this case, the desorption attempt imposes a kinetic constraint because particle removal can be rejected, whereas in the desorption method two particles are enforced to be removed. We performed these sets of simulations with and without surface diffusion. For a system with surface diffusion, after each attempt, D diffusion attempts are performed as described before. Fifteen hundred independent runs were performed to extract the success rate of adsorption attempts and to obtain the blocking function.

III. RESULTS

The determination of phase behavior and, in particular, the nature of phase transitions in two-dimensional (2D) systems is often clouded by finite-size effects and by access to the appropriate thermodynamic regime, which can bring uncertainty regarding phase behavior of the system; mainly the nature of phase transitions [11,67,70,71]. Accessing the thermodynamic regime and using sufficiently large system size to suppress errors due to finite-size effects are initial steps toward studying the phase behavior of the system [11,12,67,72]. One of the advantages of using the RSAD method is that we know how big our system should be to ensure that the results are both accurate and computationally inexpensive.

The effect of surface diffusion and system size are shown in Figs. 2(a) and 2(b). Initially, when the system is dilute, all of the curves regardless of their methods, the magnitude of surface diffusion, or the system size coincide at low surface coverage, as presented in Fig. 2(a). At high surface coverage, the probability of success of adsorbing a new particle reduces drastically due to the caging effect. However, as the ordering of particles enhances, this caging effect diminishes to maximize the available surface for accepting the incoming particles. The system reaches the equilibrium state when curves obtained from the two methods (adsorption and desorption) overlap for the entire range of fractional surface coverage, which justifies the access to the thermodynamic regime. So the results obtained from the adsorption and desorption methods are expected to bracket the correct equilibrium EOS.

To assess the role of lattice geometry, we further compared the blocking function of hard-core particles with

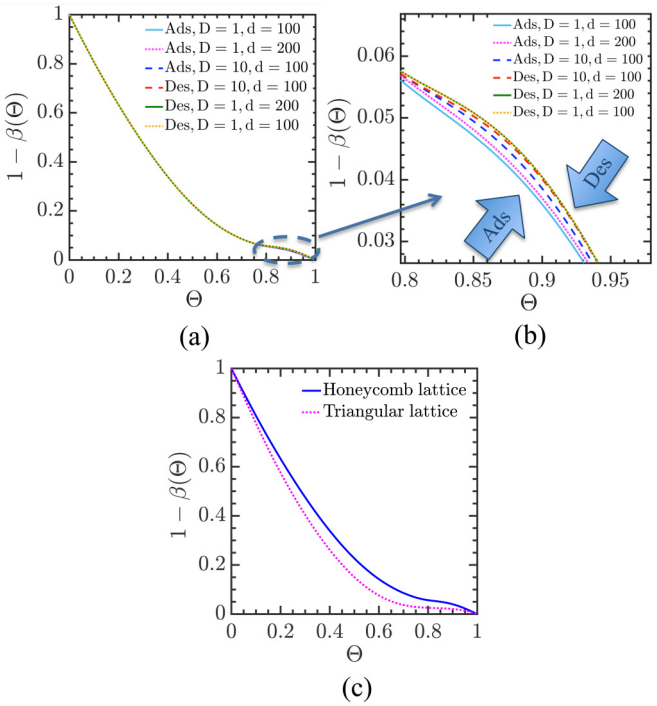

FIG. 2. (a) Effect of surface diffusion and lattice size on success rate of adsorption. "Ads" and "Des" refer to adsorption and desorption methods, respectively. (b) The inset magnifies the high-coverage region to better show the sensitivity of the blocking function to surface diffusion and lattice size. (c) Comparison of the blocking function of the honeycomb with the triangular lattice [66].

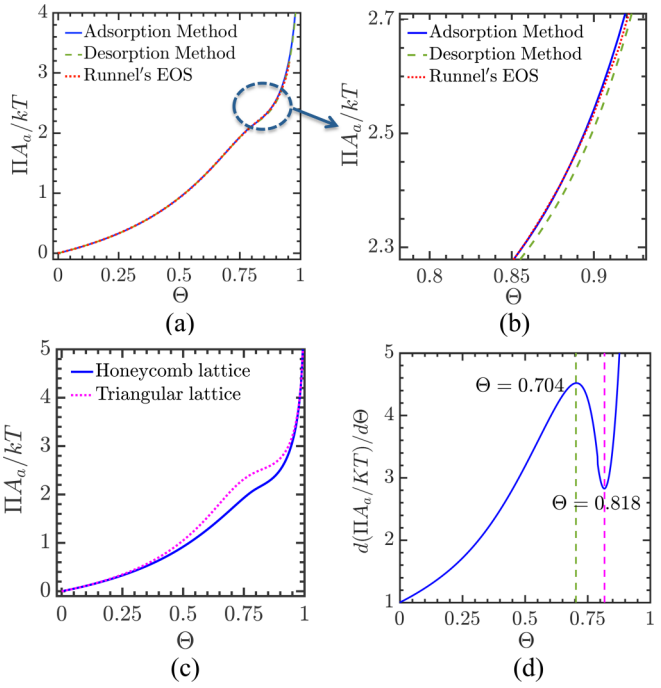

FIG. 3. (a) Comparison between our EOS where $d = 100$ and $D = 10$ with Runnels *et al.* (exact finite matrix method) [47] for hard-core molecules on a honeycomb lattice. (b) The inset shows a magnified view of the EOS in the phase-transition region. (c) Comparison between the EOS of honeycomb and triangular lattices. A_a for the honeycomb and triangular lattices are two and three, respectively. (d) Analysis of phase-transition region of honeycomb lattice based on derivative of surface pressure of desorption method with respect to surface coverage ($d = 100$ and $D = 10$).

first-neighbor exclusion on a honeycomb lattice with those on a triangular lattice [66] in Fig. 2(c). Owing to extra lattice spacing between adjacent sites in the honeycomb lattice, the lower blocking function is obtained over adsorption of particles compared with the triangular lattice.

The EOS and phase transition of hard-core molecules with the first neighbor exclusion on a honeycomb lattice were studied with various statistical mechanical approaches [34,47,73–75]. Runnels *et al.* [47] used an exact finite matrix method based on a sequence of exact solutions for lattices of infinite length and increasing finite width. The results show that, far from the transition zone, convergence occurs rapidly; while in the transition region, thermodynamic properties such as density and pressure are functions only of lattice width, which can be extrapolated to infinite width, giving the second-order transition at critical density and surface pressure of 0.845 ± 0.02 and 2.24 ± 0.1, respectively. Debierre *et al.* [73] used a phenomenological renormalization method to obtain a second-order transition at a fractional surface coverage and surface pressure of 0.83 ± 0.01 and 2.20 ± 0.02, respectively. Baxter [74] found the critical component of hard-core particles on a honeycomb lattice by using a corner transfer matrix and obtained a second-order transition at a surface coverage of 0.844. Poland [75] used high density and the Padé approximation to obtain the second-order phase transition at a surface coverage of 0.822 and a surface pressure of 2.164 and 2.178 for low- and high-density series, respectively.

Although all of these methods share similarities regarding the second-order nature of the phase transition, there is no consensus on the critical value of surface coverage at the transition. Our results have been compared with the analytical calculation of Runnels *et al.* [47] for $d = 100$ and $D = 10$ in Figs. 3(a) and 3(b). As illustrated in Fig. 3(a), at low surface coverage there is no difference between the reported equations of state. However, in the vicinity of the phase transition, a slight difference is observed [see Fig. 3(b)]. Runnels' EOS follows the *adsorption method* at a lower limit of surface coverage of the transition region and the *desorption method* at a higher limit of surface coverage of the transition region. Eventually, all of the EOSs coincide as they approach the maximum packing coverage.

Comparing the EOS of the honeycomb lattice with that of the triangular lattice [66] in Fig. 3(c) shows that, initially, both equations of state overlap at low surface coverage. As the surface coverage increases, triangular lattice shows higher surface pressure in the vicinity of the phase transition. Close to the maximum packing, finding the vacant site becomes the only determinant factor; consequently, all of the equation of states obey the Langmuir model and both lattice geometries display the same surface pressure.

The phase-transition zone of the honeycomb lattice is examined in more detail by taking the derivative of the surface pressure with respect to surface coverage, as displayed in Fig. 3(d). A second-order phase transition is obtained, which is in agreement with others [34,47,73–75], where the critical exponents obtained by Debierre *et al.* [73] and others [34,47]

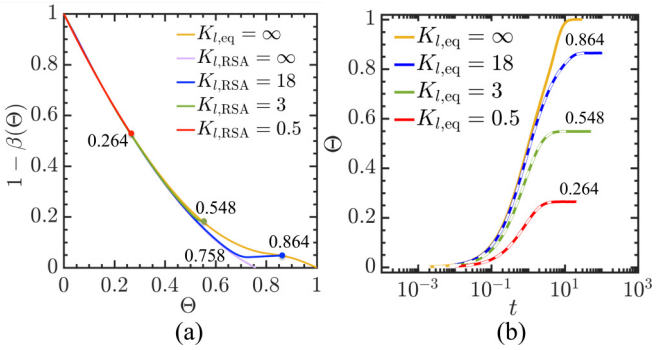

FIG. 4. (a) Blocking function for different $K_{l,\mathrm{RSA}}$ where $d = 100$ and $D = 0$. Filled dots show the equilibrium values of surface coverage. (b) Time evolution of fractional surface coverage for different $K_{l,eq}$ where $d = 100$ and $D = 10$ in the presence of surface diffusion. White dashed lines are obtained from the prediction of the RSAD model.

suggest that this system belongs to the 2D Ising universality class. The onset of deviation from the liquid regime starts at $\Theta = 0.704$ and the system solidifies at $\Theta = 0.818$ and a surface pressure of 2.169 ± 0.002, where the adsorption and desorption methods set the upper and lower limit, respectively. Our results are in a good agreement with Poland [75]. Although the honeycomb and triangular lattices both display a second-order phase transition, the triangular lattice deviates at the lower surface coverage $\Theta = 0.652$ from the liquid regime and undergoes solidification at the higher surface coverage $\Theta = 0.827$, exhibiting a wider window of phase transition [66].

Systems with desorbing particles reach the equilibrium state below the maximum packing, as evinced in many experimental studies [15]. We explored the role of desorption for a system in equilibrium (high surface diffusion), revealing that, for different values of $K_{l,eq}$, the blocking function obtained is the same as the one predicted by Eq. (6) [$K_{l,eq} = \infty$ in Fig. 4(a)] until the steady-state value is achieved. The solid circles in Fig. 4(a) denote the steady-state surface coverage for the specified values of $K_{l,eq}$. Additionally, by plugging the blocking function obtained from Eq. (6) back into Eq. (5), we were able to obtain the time evolution of surface coverage for a given value of $K_{l,eq}$. These intriguing result are in excellent agreement with the simulation results [see white dashed lines in Fig. 4(b)]. Note that our simulations are performed on a homogeneous surface. However, surface heterogeneity can arise, for example, due to the variation in adsorption energy, nonuniform arrangement of the surface, etc., which could lead to various structural ordering on the substrate [76,77].

In the absence of surface diffusion and for $K_{l,\mathrm{RSA}} = \infty$ (corresponding to a system with no desorption), the system will reach the jamming state at the fractional surface coverage of 0.758, as illustrated in Fig. 4(a). The jamming limit in RSA is strongly dependent on the initial configuration [13]. In the absence of surface diffusion, dynamics of adsorption, which can be described with a RSA model, pushes the system toward a locked or metastable configuration. Ordering is necessary to unlock this configuration, which is a slow process and can be mediated by detachment and reattachment of the particles [36]. Figure 4(a) shows that, at the given fractional surface coverage, a larger surface is available in the equilibrium state compared with the RSA configuration [78].

For the RSA with desorption, the adsorption process is dominant at the early stage and increasing the equilibrium rate constant results in the faster crowding of the surface. For small values of $K_{l,\mathrm{RSA}}$ and when the surface is dilute, the blocking function exactly overlaps with the equilibrium blocking function curve [see red curve in Fig. 4(a)] [78–80]. However, for intermediate values of $K_{l,\mathrm{RSA}}$ [e.g., green curve in Fig. 4(a)], the system rapidly gets crowded while following the RSA curve and then slowly relaxes toward equilibrium with the higher surface coverage [14,16] where the insertion probability monotonically decreases by the increase of coverage [80].

For the system where the surface coverage surpasses the jamming coverage [see, for example, the blue curve for $K_{l,\mathrm{RSA}} = 18$ in Fig. 4(a)], the initial dominant adsorption process follows the RSA model and densifies the system in a very irregular fashion, making the deposition of a new particle very hard. At the late stage of the process, the desorption plays a significant role and the success rate of adsorption shows an interesting trend in which after the initial abrupt decline, it increases very slowly with the increase of surface coverage, indicating a higher success rate of adsorption at a higher surface coverage. Note that the blocking function eventually reaches a steady-state value identical to the equilibrium value. In the presence of desorption, the equilibrium rate constant K_l determines the equilibrium coverage while surface diffusion speeds up the process of reaching the equilibrium coverage without affecting the final value of coverage [14].

RSA with desorption shares qualitative similarities with many phenomenological properties of supercooled liquids and glasses. For instance, as the $K_{l,\mathrm{RSA}} \to \infty$, the system gets trapped in a metastable state and will not be able to relax toward the equilibrium. At high yet finite values of the equilibrium rate constant, the early stage of this process suggests a mechanism similar to a quenched disorder which leads to the formation of a supercooled liquid with a frustrated structure. This analogy with supercooled liquid appearing at the early state could be signaling the occurrence of aging phenomena at the late stage of the process. The aging phenomena is due to the strong memory effect originating from the high correlation with the initial configuration of the system where the relaxation evolves very slowly [81]. To quantify this out-of-equilibrium system and further validate our hypothesis regarding the aging process, we calculate the two-time density-density correlation function [69,82]:

$$C(t, t_w) = \frac{\langle \Theta(t)\Theta(t_w)\rangle - \langle \Theta(t)\rangle\langle \Theta(t_w)\rangle}{\langle \Theta(t_w)^2\rangle - \langle \Theta(t_w)\rangle^2}, \quad t \geqslant t_w. \tag{7}$$

Angular brackets indicate an ensemble average, and t_w is the waiting time of sampling. Out of equilibrium, $C(t, t_w)$ depends on both t and t_w.

The aging properties of RSA with desorption for $K_{l,\mathrm{RSA}} = 100$ is shown in Fig. 5. The insertion probability of this system falls below the $K_{l,\mathrm{RSA}} = 18$ in Fig. 4(a) but follows the same trend. Figure 5(b) shows the disorder configuration of the system corresponding to a state in which the insertion probability stops decaying. As the coverage slowly increases and the desorption process picks up, the degree of freedom in

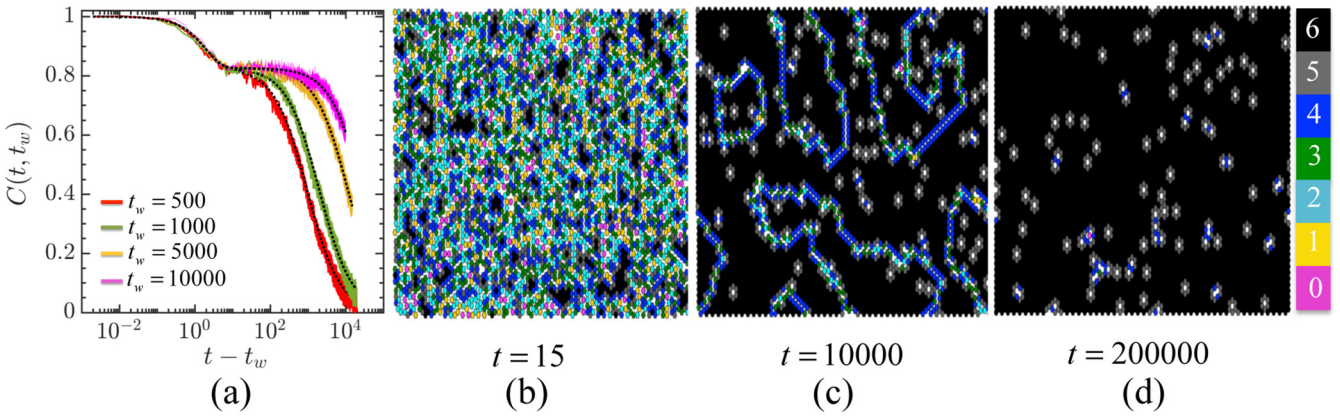

FIG. 5. (a) Two-time density-density correlation function at different t_w where $D = 0$, $d = 100$, $K_{l,\mathrm{RSA}} = 100$. The black dotted lines are obtained from Eq. (8). (b) The heatmap plot of the number of contacting neighboring sites for a system with $K_{l,\mathrm{RSA}} = 100$ at different temporal surface coverages of (b) $\Theta = 0.7532$, (c) $\Theta = 0.9459$, (d) $\Theta = 0.979$. The color bar identifies the number of contacting neighbors.

the system enhances and the decorrelation occurs due to the unlocking of the frustrated structure. As the degree of ordering in the system enhances, which is evinced by the formation of clusters [see black clusters in Figs. 5(c) and 5(d)], the $C(t, t_w)$ curve shows an interesting trends where it follows the unique curve [see black dotted lines in Fig. 5(a)], which can be fit with the following equation:

$$C(t, t_w) = (1 - q)\exp\left[-\alpha(t - t_w)\right] + q\left(\frac{t_w + t_s}{t + t_s}\right), \quad (8)$$

where q, α, and t_s are fitting parameters. The constant q increases by increasing the $K_{l,\mathrm{RSA}}$ and t_s is approximately equal to t_w. Figure 5(a) shows that the correlation function follows two times sectors. Initially all of the correlation curves decay to a nonzero plateau and follow the stationary exponential term in Eq. (8).

The exponential term in Eq. (8) is related to localized motion of particles within the cage, which facilitates fast filling of the vacant sites and obeys time-translation invariance independent of t_w [83,84]. Then, the correlation curves decay from this plateau to zero and follow the power-law term (with exponent -1) in Eq. (8). The second decay depends on the waiting time and is called simple aging because it follows the power law. As the waiting time increases, the decorrelation takes longer, suggesting that cages are stiffer [81]. The second term implies the structural relaxation and appearance of cluster coarsening in the system where clusters merge by increasing t_w [83]. With the passage of time, the clusters' coarsening results in the increase of insertion probability. Note that the equilibrium state [Fig. 5(d)] is less blocked than the disorder configuration [Fig. 5(b)]. Equation (8) suggests the weak-ergodicity breaking scenario where, for $t > t_w$, the correlation function decays as follows [84,85]:

$$\lim_{t\to\infty} C(t, t_w) = 0, \quad (9)$$

$$\lim_{t_w\to\infty} C(t, t_w) = (1 - q)\exp\left[-\alpha(t - t_w)\right] + q, \quad (10)$$

$$\lim_{t_w\to\infty} \lim_{t-t_w\to\infty} C(t, t_w) = q, \quad (11)$$

where q is the Edwards-Anderson order parameter which can be defined from Eq. (11) [81]. In our system, for $K_{l,\mathrm{RSA}} = 100$, we find $q = 0.8257$.

We further address the influence of system's initial state on its dynamical response to a sudden change of K_l. The following outlines the series of simulations that were performed to obtain different initial states and once the system reached the target coverage ($\Theta = 0.758$) the simulations were stopped:

$\mathcal{A}$ Starting from an empty lattice, the RSA with $K_{l2} = \infty$ was performed to achieve a glassy state with a *much higher* blocking function compared with the equilibrium.

$\mathcal{B}$ Starting from an empty lattice, the RSA were performed with a chosen value of $K_{l2} = 14$ that would result in steady-state coverage above the target coverage of $\Theta = 0.758$ to achieve a system with a blocking function *higher* than the equilibrium state.

$\mathcal{C}$ For a steady-state system with high coverage, the value of $K_{l1} = 18$ was dropped to a low value $K_{l2} = 0.5$, engendering a system with a blocking function *much smaller* than that of the equilibrium state.

$\mathcal{D}$ For a fully packed system, the value of $K_{l1} = \infty$ was dropped to $K_{l1} = 0$, leading to a system with a blocking function *much smaller* than that of the equilibrium system. Once the systems reached the target coverage from the different paths described above, the value of K_{l2} was changed to a new value $K_{l3} = 18$ [Fig. 6(a)] and $K_{l3} = 7$ [Fig. 6(b)] to study the dynamical response of the system to this stimuli.

For the glassy state $\mathcal{A}$ [see Figs. 6(a) and 6(b)], a valley appears in the coverage temporal evolution curve, where the depth of the valley depends on the value K_{l3}. For larger K_{l3}, the depth will be shallower. However, this valley will disappear for a critical small value of K_{l3} and the coverage will decrease monotonically to reach the steady-state value. The opposite behavior is observed for the system with $\mathcal{D}$ initial state by the appearance of a peak in the coverage-time plot [Figs. 6(a) and 6(b)]. However, the appearance of this peak depends on the value of K_{l3}. For $\mathcal{B}$ ($\mathcal{C}$) state, for the sudden change of K_{l2} to $K_{l3} = 18$, where the steady-state coverage is higher than the initial state, the surface coverage will smoothly (abruptly) increases to reach the steady-state value. The opposite trend is observed for the sudden change of K_{l2} to $K_{l3} = 7$. Figure 6(a)

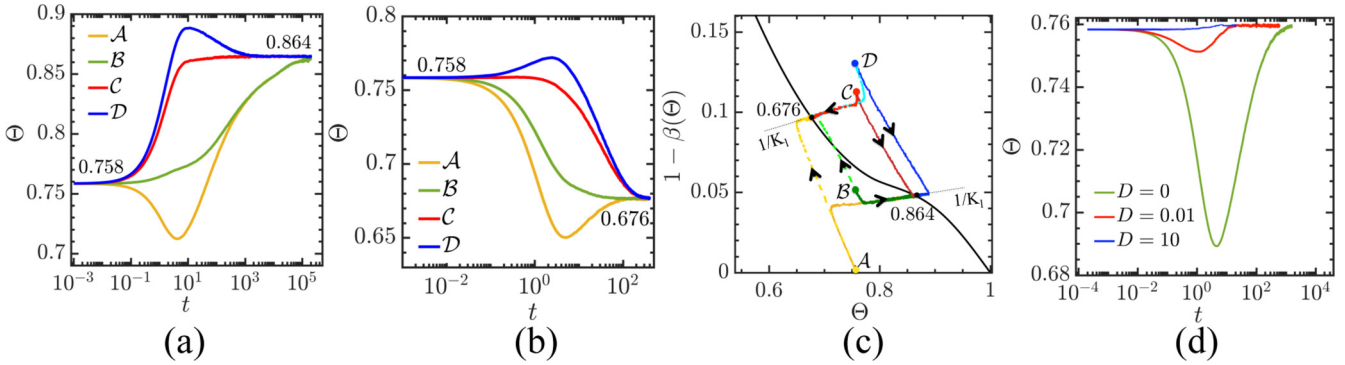

FIG. 6. Dynamical response of the system to abrupt change of K_{l2} to (a) $K_{l3} = 18$ and (b) $K_{l3} = 7$ from different initial states $\mathcal{A}$, $\mathcal{B}$, $\mathcal{C}$, and $\mathcal{D}$. (c) The insertion probability of adsorption for different initial states $\mathcal{A}$, $\mathcal{B}$, $\mathcal{C}$, and $\mathcal{D}$ due to abrupt changes of K_{l2} to $K_{l3} = 18$ and $K_{l3} = 7$ corresponding to panels (a) and (b). (d) Dynamical response of the system with initial jammed configuration to the sudden change of K_l (from ∞ to 11.62) for different values of surface diffusion.

shows that the time evolution of surface coverage, regardless of their history, overlaps after some relaxation time.

To gain a better insight into the dynamical response of the system to different initial states, we further analyze the insertion probability. Figure 6(c) displays an interesting result that there is a specific path [identified by black dashed lines in Fig. 6(c)] related to each value of K_l. If the initial state is above (below) this path, the adsorption (desorption) process is initially dominant until it crosses this path, and then there is a tug-of-war competition between adsorption and desorption along this path until the system reaches the steady-state value. If the crossing occurs on the right (left) of the equilibrium line [black line in Fig. 6(c)], the surface coverage decreases (increases) to reach the steady state. This path is encoded in the memory of the system and the system retains a strong memory of its K_l history where the slope of this path is nearly equal to the inverse of K_l.

Dynamical response of an initially jammed system to the sudden change of K_l (from ∞ to 11.62) and for different values of surface diffusion has been investigated, as shown in Fig. 6(d). The judicious choice of $K_l = 11.6$ serves to drive the system towards the steady-state coverage equal to the jamming coverage (the initial state of the simulation). This abrupt change results in the initial increase of desorption rate and consequently enhances the insertion probability of adsorption. For fast-enough surface diffusion, the system immediately reaches the steady-state configuration. However, in the absence of surface diffusion or at low values, a minimum appears in the time evolution plot of surface coverage, which is rooted in the relaxation of the caging effect.

In hard-core system, internal energy is a function only of temperature and not of density [86]. Given hard-core interactions are athermal, all of the phase transitions are entropy driven, where the ordered phase has a higher entropy than the disordered phase [34,86]. Consequently, we expect that the hysteresis between equilibrium system and its nonequilibrium counterpart comes from change in configurational entropy [87]. Therefore, the blocking function and surface coverage would be the only information required to calculate the surface pressure. To corroborate this statement, we compare the surface pressure obtained from the blocking function for two systems with the equal equilibrium rate constant of $K_l = 18$ but different surface diffusion $D = 0.01$ and $D = 10$, which are named $K_{l,neq} = 18$ and $K_{l,eq} = 18$, respectively [Figs. 7(a) and 7(b)]. The blocking functions are the same for both systems at the steady state and also at low surface coverages [see Fig. 7(a)]. As such, we expect that, at these two limits, the surface coverages overlap, the insertion of both equilibrium and nonequilibrium blocking functions [Fig. 7(a)] into Eq. (4) yields the same surface pressure. Figure 7(b) shows that the values of surface pressure at the equilibrium are exactly identical for both $K_{l,neq} = 18$ and $K_{l,eq} = 18$, which underscores the validity of our hypothesis. For systems in equilibrium, surface pressure is only a function of surface coverage, as evinced

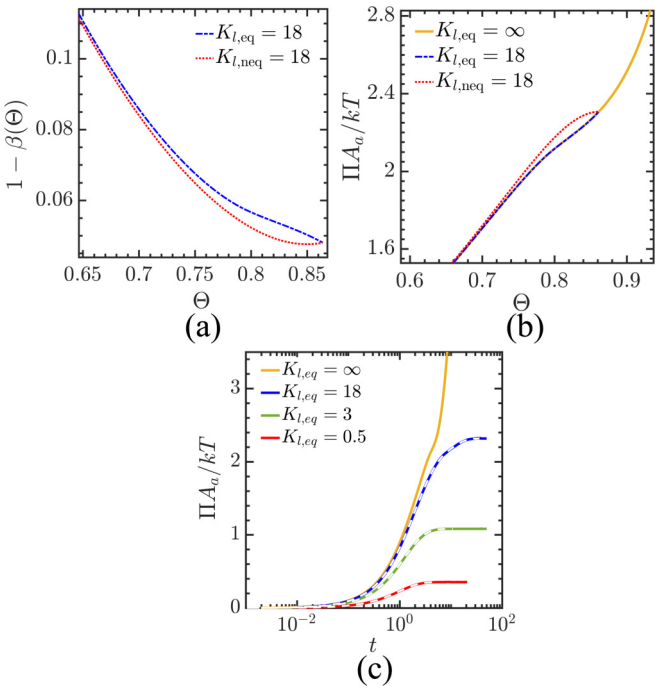

FIG. 7. (a) Success rate of adsorption for the equilibrium system $K_{l,eq} = 18$ and nonequilibrium system $K_{l,neq} = 18$ where $d = 100$. (b) Surface pressure versus surface coverage. (c) Time evolution of surface pressure for systems with various $K_{l,eq}$. White dashed lines are obtained from the prediction of the RSAD model.

by the overlap of the surface pressure curves for $K_{l,eq} = 18$ and $K_{l,eq} = \infty$. So the knowledge of blocking function of a nondesorbing system at equilibrium ($K_{l,eq} = \infty$) would be sufficient to accurately obtain the surface pressure of the equilibrium systems with various $K_{l,eq}$. Figure 7(b) further displays that the surface pressure curve of nonequilibrium system is always higher than the equilibrium one as the system becoming gradually packed, which can explain the hysteresis observed in some experiments [2]. We also compare the time evolution of equilibrium surface pressure for systems with defined $K_{l,eq}$ and the results obtained from $K_{l,eq} = \infty$. This is accomplished by inserting the blocking function obtained from Eq. (6) into Eqs. (4) and (5) and integrating to obtain the temporal evolution of surface pressures [identified by white dashed lines in Fig. 7(c)], which shows excellent agreement with the simulation results.

IV. CONCLUSION

In this paper we studied the phase behavior and adsorption kinetics of hard-core molecules with first-neighbor exclusions on a honeycomb lattice by incorporating a desorption process through a varying equilibrium rate constant in the RSAD model. Our analyses confirm earlier statistical mechanics results concerning the second-order nature of the phase transition [34,47,73–75]. We show that the system is in a liquid regime below a surface coverage of 0.704 and undergoes a second-order transition at a surface coverage of 0.818, which is in a good agreement with the work of Poland [75] who used high density and Padé approximation methods to obtain the EOS.

Comparing the results of a hard-core particle on a honeycomb lattice with the same on a triangular lattice [66] shows that the blocking function is sensitive to the lattice geometry. However, once the surface coverage and the blocking function are obtained from RSAD model, all other thermodynamic properties can be calculated from the same scheme explained in Sec. II irrespective of the lattice geometry. Higher surface pressure is obtained at intermediate surface coverage for the triangular lattice, while at low surface coverages and close to the maximum packing both lattice structures display the same surface pressure. Both lattice geometries show a second-order phase transition; however, the triangular lattice undergoes a wider range of phase transitions, meaning that it deviates from the liquid regime at a lower surface coverage and solidifies at a higher surface coverage.

For the systems with desorption processes present, all of the results related to the temporal evolution of the blocking function, surface coverage, and surface pressure for various K_l can be derived from the blocking function of a system with $K_{l,eq} = \infty$. Taken together, the RSAD model without desorption is able to accurately recover deposition dynamics results for systems with desorption.

In the absence of surface diffusion, the blocking function generated by the RSA model including desorption shows three distinct regimes. Initially, when the surface is dilute, the blocking function is identical to that in thermal equilibrium. At intermediate coverage, the blocking function initially follows the RSA model and then decreases monotonically to reach the equilibrium blocking coverage at the steady state. However, when the surface coverage surpasses the jamming coverage, the insertion probability of a new particle shows an interesting trend in which, after the initial abrupt decline, it increases very slowly with the increase of surface coverage. At steady-state and for a given value of the rate constant, the blocking function and surface coverage eventually recover the values for nondesorbing systems at equilibrium. Aging analysis of the last regime with small desorption probability through the two-time density-density correlation function shows two time sectors, where it initially follows the stationary regime and then decays as a power law. As the waiting time increases, the decorrelation takes longer, which is an indication of a stiffer cage. As time passes, the structural relaxation and clustering of particles favor more densification which leads to a lower blocking function.

Analyses of the dynamical response of the system to an abrupt change of the rate constants K_l at different initial states reveals that there is a specific path toward equilibrium for each value of K_l, where the slope of this path is almost equal to $1/K_l$. This result also explains the appearance of a peak and a valley after a sudden change of K_l to a secondary value. For a system without surface diffusion, the system retains a strong memory of its history while the presence of surface diffusion results in the rapid decorrelation of memory effects.

Hard-core systems are entropy driven, and as such the blocking function and surface coverage would be the only information required to calculate the surface pressure. We show that the equilibrium surface pressure is insensitive to the values of surface diffusion and systems in that low and high values of surface diffusion result in identical surface pressure. Out of equilibrium and as the surface coverage is gradually increased, the system shows higher surface pressure than the equilibrium one, which could explain the hysteresis reported in some experimental observations.

ACKNOWLEDGMENTS

This research was supported by the National Science Foundation under Grant No. 1743794, PIRE: Investigation of Multi-Scale, Multi-Phase Phenomena in Complex Fluids for the Energy Industries.

[1] V. Fainerman and D. Vollhardt, J. Phys. Chem. B **103**, 145 (1999).

[2] V. Pauchard, J. P. Rane, and S. Banerjee, Langmuir **30**, 12795 (2014).

[3] F. Liu, S. Darjani, N. Akhmetkhanova, C. Maldarelli, S. Banerjee, and V. Pauchard, Langmuir **33**, 1927 (2017).

[4] X. Hua, J. Frechette, and M. A. Bevan, Soft Matter **14**, 3818 (2018).

[5] Z. Hou, K. Zhao, Y. Zong, and T. G. Mason, Phys. Rev. Mater. **3**, 015601 (2019).
[6] S. Fortuna, D. L. Cheung, and A. Troisi, J. Phys. Chem. B **114**, 1849 (2010).
[7] U. K. Weber, V. M. Burlakov, L. M. A. Perdigão, R. H. J. Fawcett, P. H. Beton, N. R. Champness, J. H. Jefferson, G. A. D. Briggs, and D. G. Pettifor, Phys. Rev. Lett. **100**, 156101 (2008).
[8] V. Gorbunov, S. Akimenko, A. Myshlyavtsev, V. Fefelov, and M. Myshlyavtseva, Adsorption **19**, 571 (2013).
[9] P. Bak, P. Kleban, W. N. Unertl, J. Ochab, G. Akinci, N. C. Bartelt, and T. L. Einstein, Phys. Rev. Lett. **54**, 1539 (1985).
[10] D. E. Taylor, E. D. Williams, R. L. Park, N. C. Bartelt, and T. L. Einstein, Phys. Rev. B **32**, 4653 (1985).
[11] E. P. Bernard and W. Krauth, Phys. Rev. Lett. **107**, 155704 (2011).
[12] M. Engel, J. A. Anderson, S. C. Glotzer, M. Isobe, E. P. Bernard, and W. Krauth, Phys. Rev. E **87**, 042134 (2013).
[13] J. Talbot, G. Tarjus, and P. Viot, Phys. Rev. E **61**, 5429 (2000).
[14] I. Lončarević, L. Budinski-Petković, and S. B. Vrhovac, Phys. Rev. E **76**, 031104 (2007).
[15] S. Zarkar, V. Pauchard, U. Farooq, A. Couzis, and S. Banerjee, Langmuir **31**, 4878 (2015).
[16] R. S. Ghaskadvi and M. Dennin, Phys. Rev. E **61**, 1232 (2000).
[17] D. K. Beaman, E. J. Robertson, and G. L. Richmond, Proc. Natl. Acad. Sci. U. S. A. **109**, 3226 (2012).
[18] S.-Q. Liu, J.-J. Xu, and H.-Y. Chen, Colloids Surf., B **36**, 155 (2004).
[19] V. Fainerman, R. Miller, J. K. Ferri, H. Watzke, M. Leser, and M. Michel, Adv. Colloid Interface Sci. **123**, 163 (2006).
[20] H. Wege, J. Holgado-Terriza, A. Neumann, and M. Cabrerizo-Vılchez, Colloids Surf., A **156**, 509 (1999).
[21] V. Fainerman, M. Leser, M. Michel, E. Lucassen-Reynders, and R. Miller, J. Phys. Chem. B **109**, 9672 (2005).
[22] I. Langmuir, J. Am. Chem. Soc. **40**, 1361 (1918).
[23] J. P. Rane, S. Zarkar, V. Pauchard, O. C. Mullins, D. Christie, A. B. Andrews, A. E. Pomerantz, and S. Banerjee, Energy Fuels **29**, 3584 (2015).
[24] J. P. Rane, V. Pauchard, A. Couzis, and S. Banerjee, Langmuir **29**, 4750 (2013).
[25] E. Lucassen-Reynders, J. Phys. Chem. **70**, 1777 (1966).
[26] R. Wuestneck, R. Miller, J. Kriwanek, and H.-R. Holzbauer, Langmuir **10**, 3738 (1994).
[27] V. Fainerman, E. Lucassen-Reynders, and R. Miller, Colloids Surf., A **143**, 141 (1998).
[28] P. Joos, Biochim. Biophys. Acta, Biomembr. **375**, 1 (1975).
[29] H. C. M. Fernandes, Y. Levin, and J. J. Arenzon, Phys. Rev. E **75**, 052101 (2007).
[30] J. Kundu and R. Rajesh, Phys. Rev. E **89**, 052124 (2014).
[31] F. Sanchez-Varretti, P. Pasinetti, F. Bulnes, and A. Ramirez-Pastor, Surf. Sci. **701**, 121698 (2020).
[32] D. Mandal, T. Nath, and R. Rajesh, Phys. Rev. E **97**, 032131 (2018).
[33] G. A. Iglesias Panuska, P. M. Centres, and A. J. Ramirez-Pastor, Phys. Rev. E **102**, 032123 (2020).
[34] F. C. Thewes and H. C. M. Fernandes, Phys. Rev. E **101**, 062138 (2020).
[35] A. Cadilhe, N. Araújo, and V. Privman, J. Phys.: Condens. Matter **19**, 065124 (2007).
[36] E. Frey and A. Vilfan, Chem. Phys. **284**, 287 (2002).
[37] Z. Adamczyk, Curr. Opin. Colloid Interface Sci. **17**, 173 (2012).
[38] J. J. Ramsden, J. Phys. Chem. **96**, 3388 (1992).
[39] V. Privman, *Annual Reviews Of Computational Physics III* (World Scientific, Singapore, 1995), pp. 177–193.
[40] S. Ji, C. Ates, and I. Lesanovsky, Phys. Rev. Lett. **107**, 060406 (2011).
[41] M. Lackinger, S. Griessl, T. Markert, F. Jamitzky, and W. M. Heckl, J. Phys. Chem. B **108**, 13652 (2004).
[42] Y. Zhang, V. Blum, and K. Reuter, Phys. Rev. B **75**, 235406 (2007).
[43] R. J. Baxter, *Exactly Solved Models in Statistical Mechanics* (Courier Corp., North Chelmsford, MA, 2007).
[44] A. Bellemans and R. Nigam, J. Chem. Phys. **46**, 2922 (1967).
[45] J. Orban and A. Bellemans, J. Chem. Phys. **49**, 363 (1968).
[46] F. H. Ree and D. A. Chesnut, J. Chem. Phys. **45**, 3983 (1966).
[47] L. Runnels, L. Combs, and J. P. Salvant, J. Chem. Phys. **47**, 4015 (1967).
[48] L. Runnels and L. Combs, J. Chem. Phys. **45**, 2482 (1966).
[49] X. Feng, H. W. Blöte, and B. Nienhuis, Phys. Rev. E **83**, 061153 (2011).
[50] Z. Rotman and E. Eisenberg, Phys. Rev. E **80**, 031126 (2009).
[51] D. S. Gaunt and M. E. Fisher, J. Chem. Phys. **43**, 2840 (1965).
[52] D. S. Gaunt, J. Chem. Phys. **46**, 3237 (1967).
[53] E. Eisenberg and A. Baram, Europhys. Lett. **71**, 900 (2005).
[54] M. V. Ushcats, Phys. Rev. E **91**, 052144 (2015).
[55] M. V. Ushcats, L. A. Bulavin, V. M. Sysoev, and S. J. Ushcats, Phys. Rev. E **94**, 012143 (2016).
[56] E. Cowley, J. Chem. Phys. **71**, 458 (1979).
[57] D. Burley, Proc. Phys. Soc., London **75**, 262 (1960).
[58] H. Hansen-Goos and M. Weigt, J. Stat. Mech. Theor. Exp. (2005) P04006.
[59] K. Binder and D. P. Landau, Phys. Rev. B **21**, 1941 (1980).
[60] D. A. Chesnut, J. Comput. Phys. **7**, 409 (1971).
[61] D.-J. Liu and J. W. Evans, Phys. Rev. B **62**, 2134 (2000).
[62] H. C. M. Fernandes, J. J. Arenzon, and Y. Levin, J. Chem. Phys. **126**, 114508 (2007).
[63] T. Nath and R. Rajesh, Phys. Rev. E **90**, 012120 (2014).
[64] G. S. Rushbrooke and H. I. Scoins, Proc. R. Soc. London A **230**, 74 (1955).
[65] L. Lafuente and J. A. Cuesta, Phys. Rev. E **68**, 066120 (2003).
[66] S. Darjani, J. Koplik, and V. Pauchard, Phys. Rev. E **96**, 052803 (2017).
[67] S. Darjani, J. Koplik, S. Banerjee, and V. Pauchard, J. Chem. Phys. **151**, 104702 (2019).
[68] J. W. Evans, Rev. Mod. Phys. **65**, 1281 (1993).
[69] M. Nicodemi and A. Coniglio, Phys. Rev. Lett. **82**, 916 (1999).
[70] C. H. Mak, Phys. Rev. E **73**, 065104(R) (2006).
[71] K. Wierschem and E. Manousakis, Phys. Rev. B **83**, 214108 (2011).
[72] W. Zhang and Y. Deng, Phys. Rev. E **78**, 031103 (2008).
[73] J.-M. Debierre and L. Turban, Phys. Lett. A **97**, 235 (1983).
[74] R. Baxter, Ann. Comb. **3**, 191 (1999).
[75] D. Poland, Phys. Rev. E **59**, 1523 (1999).
[76] F. O. Sanchez-Varretti, F. M. Bulnes, and A. J. Ramirez-Pastor, Adsorption **25**, 1317 (2019).
[77] W. J. Ceyrolles, P. Viot, and J. Talbot, Langmuir **18**, 1112 (2002).

[78] X. Jin, J. Talbot, and N.-H. L. Wang, AIChE J. **40**, 1685 (1994).
[79] J. Talbot, X. Jin, and N.-H. Wang, Langmuir **10**, 1663 (1994).
[80] G. Tarjus, P. Schaaf, and J. Talbot, J. Chem. Phys. **93**, 8352 (1990).
[81] L. F. Cugliandolo, in *Course 7: Dynamics of Glassy Systems Slow Relaxations and Nonequilibrium Dynamics in Condensed Matter (Les Houches)*, edited by J. L. Barrat, M. Feigelman, J. Kurchan, and J. Dalibard (Springer, Berlin, Heidelberg, 2003), Vol. 77, pp. 367–521.
[82] J. Šćepanović, D. Stojiljković, Z. Jakšić, L. Budinski-Petković, and S. Vrhovac, Phys. A (Amsterdam, Neth.) **451**, 213 (2016).
[83] F. Ritort and P. Sollich, Adv. Phys. **52**, 219 (2003).
[84] A. J. Kolan, E. R. Nowak, and A. V. Tkachenko, Phys. Rev. E **59**, 3094 (1999).
[85] L. F. Cugliandolo and J. Kurchan, Phys. Rev. Lett. **71**, 173 (1993).
[86] D. Frenkel, Phys. A (Amsterdam, Neth.) **263**, 26 (1999).
[87] T. M. Nieuwenhuizen, Phys. Rev. Lett. **80**, 5580 (1998).